NASA Technical Paper 2294

April 1984

Analysis of a Topping-Cycle, Aircraft, Gas-Turbine-Engine System Which Uses Cryogenic Fuel

George E. Turney and
Laurence H. Fishbach

NASA

NASA
Technical
Paper
2294

1984

Analysis of a Topping-Cycle, Aircraft, Gas-Turbine-Engine System Which Uses Cryogenic Fuel

George E. Turney and
Laurence H. Fishbach

Lewis Research Center
Cleveland, Ohio

NASA
National Aeronautics
and Space Administration

Scientific and Technical
Information Branch

Summary

An analytical investigation was made of a topping-cycle aircraft engine system that uses a cryogenic fuel. This system consists of a main turboshaft engine mechanically coupled (by cross-shafting) to a topping loop, which augments the shaft power output of the system.

The thermodynamic performance of the topping-cycle engine was analyzed and compared with that of a reference or baseline turboshaft engine which was operated under the same cycle conditions. For the cycle operating conditions selected, the performance (i.e., thermal efficiency and/or specific fuel consumption) of the topping-cycle engine was determined to be about 12 percent better than that of the reference turboshaft engine.

Engine weight estimates were made for both the topping-cycle engine and the baseline turboshaft engine. These estimates were based on a common shaft power output for each engine. Results indicate that the topping-cycle engine weight is comparable with that of the baseline turboshaft engine.

Introduction

The problem of meeting the nation's energy needs in the coming years has become a subject of increasing concern. In the area of air transportation NASA and others have studied the possible use of fuels other than the usual petroleum-derived hydrocarbons. Two of the alternative fuels that have received attention are cryogenics, namely, liquid hydrogen (LH_2) and liquid methane (LCH_4). References 1 and 2 report on the future needs for alternative fuels and point out some of the considerations involved with the use of liquid hydrogen and liquid methane as commercial air transport fuels.

Liquid hydrogen and liquid methane have been studied extensively as alternative fuels for both subsonic and supersonic transport aircraft (refs. 3 and 4, e.g.). The pros and cons associated with these fuels are well recognized. Storage and handling are considered to be primary drawbacks. The high heating value of these fuels is the main reason for their consideration. Their cryogenic state can also allow them to be used effectively as heat sinks to reduce or eliminate the use of compressor bleed air for turbine cooling.

In reference 5 other schemes for improving engine performance are described, such as using cryogenic fuel as a heat sink to precool the compressor airflow, expanding heated fuel through an auxiliary turbine to produce additional shaft work, and preheating a portion of the fuel before burning it in a combustor.

In this report, a topping-cycle gas-turbine engine is introduced which combines all of these mentioned schemes for improving engine brake specific fuel consumption (bsfc). This engine (hereafter referred to as the "topping-cycle engine") consists of a main turboshaft engine augmented by a direct-coupled secondary power generation loop (topping loop). The topping loop operates with precooled compressor air and a fuel-rich combustor. The fuel-rich combustion products are expanded through an auxiliary turbine in this loop and are then fed into the burner of the main turboshaft engine where the excess fuel is burned completely. The topping-cycle engine concept was originally proposed by Mr. Robert W. Schroeder, now retired and formerly chief of the V/STOL and Noise Division at the Lewis Research Center.

The study presented in this report deals primarily with the thermodynamic performance characteristics of this engine system. As a part of this study, assessments were also made of the weight associated with this engine system. Results of the thermodynamic analysis and the engine weight analysis are described in this report.

This engine study is based on the use of liquid hydrogen fuel. However, in principle, the topping-cycle engine could operate with other cryogenic fuels, such as liquid methane.

Description of Topping-Cycle Engine

As an aid in understanding the topping-cycle engine, consider first a simplified version of a hydrogen fueled turboshaft engine (e.g., fig. 1). Air entering this engine is compressed by the compressor (C1), is mixed with the hydrogen fuel pumped from the storage tank, and is burned. The combustion products are expanded through the turbine to produce work. The work produced by the turbine drives the main compressor and fuel pump and also powers an external load. The external load in this system could be a fan, a propeller or some other propulsive component.

Figure 2 shows the same turboshaft engine with a topping loop added. In this system a fraction of the compressor airflow from the main engine is bled off at an interstage point and fed to the topping loop. The topping loop in this system operates as an auxiliary power unit. The bleed air entering this loop is precooled and compressed in two separate processes. Precooling is accomplished with hydrogen-to-air heat exchangers (HX-1 and -2). Precooling is advantageous in that it reduces the compression work.

The total engine fuel flow is fed directly into the topping loop burner. The topping loop burner operates in a highly fuel rich state, with an equivalence ratio (ER) ranging somewhere between about 2.5 and 4.5. The equivalence ratio is defined as follows:

$$\text{Equivalence ratio (ER)} = \frac{\text{actual fuel-to-air ratio}}{\text{stoichiometric fuel-to-air ratio}}$$

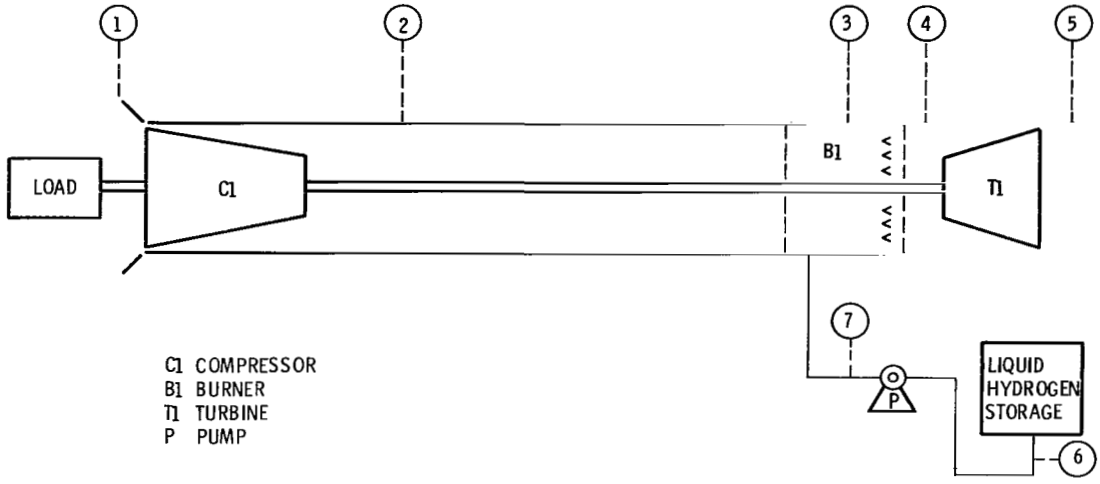

Figure 1. – Baseline hydrogen-fueled turboshaft engine.

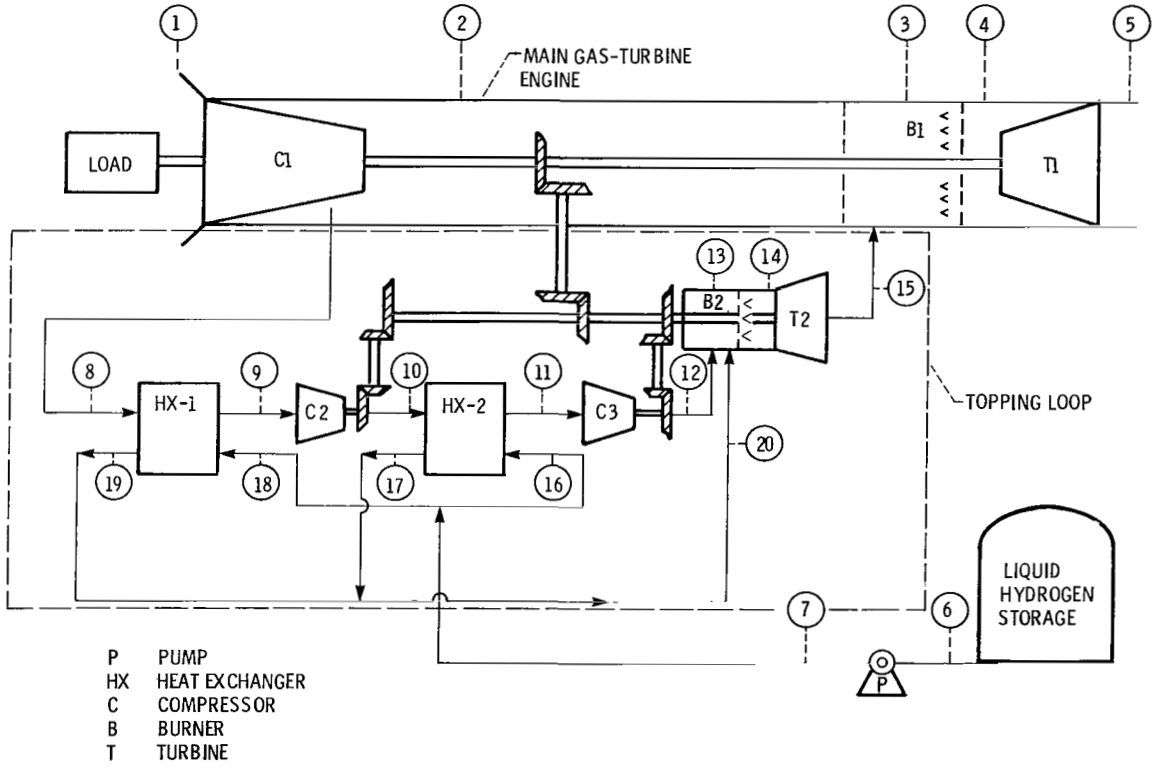

Figure 2. – Hydrogen-fuel topping-cycle engine.

Thus, only a fraction of the total fuel flow is burned in the topping loop.

The combustion products from the topping loop include hydrogen—the unburned fuel, nitrogen, and water vapor. (All oxygen is consumed in the fuel-rich burning process.) The fuel-rich combustion products are expanded through the topping-loop turbine and ducted directly into the main engine burner. There, the fuel mixture is combined with the remaining air from the main engine, burned completely, and expanded through the main engine turbine. Typically, the main engine burner operates at an equivalence ratio (ER) ranging from about 0.2 to 0.5.

As indicated in figure 2, the topping loop and the main turboshaft engine are interconnected by a crossshaft so that power produced by the topping loop turbine is supplied to the compressors and to the main engine load. Thus, the topping loop operates as an auxiliary powerplant and produces additional power which is transferred to the system load. The performance benefits of this cycle are described in the RESULTS section of this report.

Analytical Approach

The primary purpose of this study was to evaluate and assess the thermodynamic performance of the topping-cycle engine. But, in addition to the thermodynamic or cycle analysis, engine component and system weights were also evaluated.

As a first step in the approach to this study, a baseline engine was established to serve as a standard by which the topping-cycle engine could be compared. The baseline engine is the hydrogen fueled turboshaft engine depicted in figure 1 and described in the preceding section.

For the thermodynamic analysis, analytical models representing both the baseline engine (fig. 1) and the topping-cycle engine (fig. 2) were developed. All engine performance calculations for this study were based on cruise flight conditions at Mach 0.80 at an altitude of 10 668 m (35 000 ft).

To systematically evaluate the thermodynamic performance of the topping-cycle engine, appropriate equations were developed for both the topping-cycle and baseline engines. Digital codes were then formulated for calculating the performance characteristics of these engines. Fluid thermodynamic properties for the analysis were taken from three sources: Properties for parahydrogen, nitrogen, and oxygen were taken from reference 6; and properties for air and steam were obtained from references 7 and 8.

For the purpose of estimating engine system weights, a digital computer code, called WATE-2 (ref. 9), was used. This program is capable of estimating weights and dimensions of individual components (such as compressors, turbines, burners, etc.) as well as total engine system weights. The WATE-2 program was used in this study to estimate weights of both the baseline engine and the topping-cycle engine. A reference shaft power output of 7460 kW (10 000 hp) was assumed for estimating and comparing the weights of these engine systems.

THERMODYNAMIC ANALYSIS

Cycle conditions and component characteristics

Cycle operating conditions and component characteristics were established for the purpose of providing a consistent set of reference conditions for use in computing and comparing the performance of the baseline engine and topping-cycle engine. Table I is a listing of the assumed cycle operating conditions (design point conditions) and the component characteristics. As indicated in this table all components common to both of these engines (such as inlets, compressors, burners, and turbines) have identical characteristic values. The component efficiencies listed in table I are representative of current aircraft engine technology.

Figure 3 is a temperature-entropy diagram for the topping-cycle engine operating at the assumed design point conditions of table I. The pressures and temperatures at each of the major points throughout this engine are shown. As indicated, both burners in this engine system operate at a design point temperature level of 1667 K (3000° R). This temperature level is representative of an advanced technology engine.

The bleed air entering the topping loop is taken from an interstage point of compressor C1. The pressure of the bleed air was assumed to have a design value of of 5.59×10^5 Pa (81.0 psia). This pressure level was chosen to provide nearly equal heat transfer rates in the individual heat exchangers of the topping loop.

In the analysis of this engine system, a pressure matching constraint was imposed such that the exhaust stream pressure from turbine T2 was equal to the stream pressure in the main engine burner B1.

Cycle Analysis

Normally, in cycle analyses the conventional index used in rating the performance of aircraft propulsion systems is the specific fuel consumption. For turboshaft engines, such as the baseline and the topping-cycle engines, brake specific fuel consumption (*bsfc*) is used and is defined as

$$bsfc = \frac{\text{fuel flow rate}}{\text{net shaft power delivered to load}} = \frac{W_f}{SP} \tag{1}$$

(All symbols are defined in appendix A.)

Another index used to indicate aircraft propulsion system performance is the thermal efficiency, η, which is related to *bsfc*. For turboshaft engines the thermal efficiency is defined as

$$\eta = \frac{\text{net shaft power delivered to load}}{\text{chemical energy input}} = \frac{SP}{KW_f \Delta H_{comb}} \tag{2}$$

In equations (1) and (2) the net shaft power delivered to the load, *SP*, represents the total turbine power developed less the power absorbed by the compressor (or compressors) and pump. For the baseline engine (fig. 1), the net shaft power delivered to the load is

$$\begin{pmatrix}\text{Baseline engine } SP\end{pmatrix} = \begin{pmatrix}\text{power developed by turbine Ti}\end{pmatrix} - \begin{pmatrix}\text{power consumed by compressor C1}\end{pmatrix} - \begin{pmatrix}\text{power consumed by pump P}\end{pmatrix} \tag{3}$$

Or, in terms of the respective flow rates and enthalpies, equation (3) becomes

$$\begin{pmatrix}\text{Baseline engine } SP\end{pmatrix} = K[(W_a + W_f)(H_4 - H_5) - W_a(H_2 - H_1) - W_f(H_7 - H_6)] \tag{4}$$

TABLE I. – DESIGN-POINT OPERATING CONDITIONS AND COMPONENT CHARACTERISTICS FOR BASELINE ENGINE AND TOPPING-CYCLE ENGINE

[Flight conditions: Mach 0.8; 10 668 m (35 000 ft).]

Component or cycle parameter	Baseline engine	Topping cycle engine
Inlet recovery, P_1/P_o	1.0	1.0
Burner temperatures, K (°R):		
Burner B_1, T_4	1667 (3000)	1667 (3000)
Burner B_2, T_{14}	----------	1667 (3000)
Efficiencies:		
Hydrogen pump P	0.60	0.60
Main compressor C1	0.88	0.88
Compressor C2	----------	0.88
Compressor C3	----------	0.88
Main turbine T1	0.86	0.86
Turbine T2	----------	0.86
Burner B1	1.0	1.0
Burner B2	1.0	1.0
Component pressure ratios:		
Main compressor C1, P_2/P_1	43.5	43.5
Compressor C2, P_{10}/P_9	----------	6.1
Compressor C3, P_{12}/P_{11}	----------	6.1
Burner B1, P_4/P_3	0.95	0.95
Burner B2, P_{14}/P_{13}	----------	0.95
Fuel storage (saturation liquid):		
Pressure, P_6, Pa (psia)	1.01×10^5 (14.696)	1.01×10^5 (14.696)
Temperature, T_6, K (°R)	20.34 (36.608)	20.34 (36.608)
Bleed air pressure, P_8, Pa (psia)	----------	5.59×10^5 (81.0)
Inlet temperature, K (°R):		
Compressor C2, T_9	----------	333 (600)
Compressor C3, T_{11}	----------	333 (600)
Turbine T1 discharge pressure, P_5, Pa (psia)	3.64×10^4 (5.27)	3.64×10^4 (5.27)
Heat exchanger pressure ratios:		
Air side, P_9/P_8 and P_{11}/P_{10}	----------	0.99
Hydrogen side, P_{17}/P_{16} and P_{19}/P_{18}	----------	0.99

And for the topping-cycle engine (fig. 2), the net shaft power delivered to the load is

$$\begin{pmatrix}\text{Topping cycle engine } SP\end{pmatrix} = \begin{pmatrix}\text{power developed by turbine T1}\end{pmatrix} + \begin{pmatrix}\text{power developed by turbine T2}\end{pmatrix} - \begin{pmatrix}\text{power consumed by compressor C1}\end{pmatrix} - \begin{pmatrix}\text{power consumed by compressor C2}\end{pmatrix} - \begin{pmatrix}\text{power consumed by compressor C3}\end{pmatrix} - \begin{pmatrix}\text{power consumed by pump P}\end{pmatrix} \quad (5)$$

Expressed in terms of the respective flow rates and enthalpies, equation (5) becomes

$$\begin{pmatrix}\text{Topping cycle engine } SP\end{pmatrix} = K[(W_a+W_f)(H_4-H_5) + (W_{bl}+W_f)(H_{14}-H_{15}) - (W_a-W_{bl})(H_2-H_1) - W_{bl}(H_8-H_1) - W_{bl}(H_{10}-H_9) - W_{bl}(H_{12}-H_{11}) - W_f(H_7-H_6)] \quad (6)$$

Some of the enthalpy terms in equations (4) and (6) represent a weighted average for two or more component fluids. For example, the enthalpy at flow station 14 (H_{14}) is the average enthalpy per pound of fluid mixture containing nitrogen, hydrogen, and water vapor. The enthalpy of the mixture is dependent on the composition of the mixture. An appropriate expression was used to compute the enthalpy per unit mass of mixture. In equation form, the enthalpy of a unit mass of fluid consisting of a mixture of n component gases is

$$H_{mix} = \frac{\sum_{i=\text{component 1}}^{i=\text{component } n} (W_iH_i)}{\sum_{i=\text{component 1}}^{i=\text{component } n} (W_iH_i)} \quad (7)$$

In table II, a qualitative list is shown of the component fluids present at each of the respective flow stations in both the baseline and topping-cycle engines.

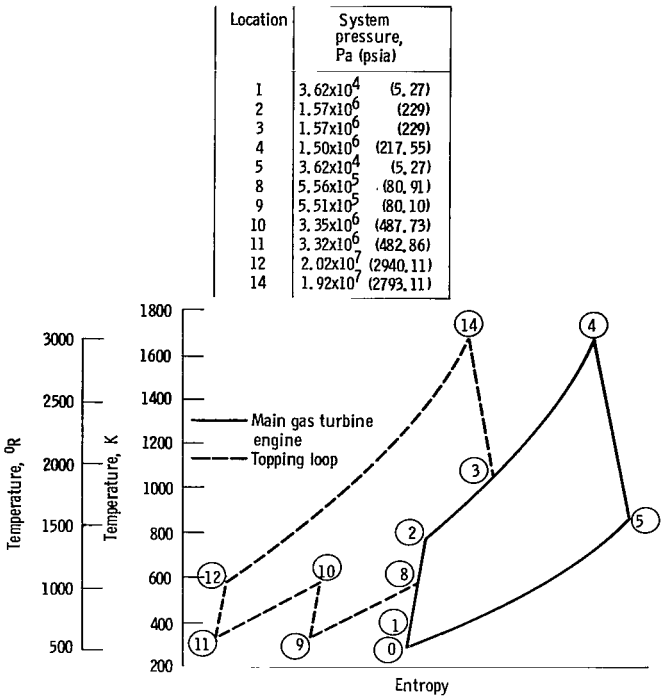

Figure 3. – Temperature-entropy illustration for topping-cycle engine. (See fig. 2 for engine locations).

TABLE II. – QUALITATIVE LIST OF COMPONENT FLUIDS AT RESPECTIVE FLOW STATIONS IN BASELINE AND TOPPING-CYCLE ENGINES[a]

Flow station	Component fluids	
	Baseline engine	Topping-cycle engine
1	Air	Air
2	Air	Air
3	Air, H_2	Air, H_2, N_2, H_2O
4	Air, N_2, H_2O	Air, N_2, H_2O
5	Air, N_2, H_2O	Air, N_2, H_2O
6	H_2	H_2
7	H_2	H_2
8–12	----------	Air
13	----------	Air, H_2
14	----------	H_2, N_2, H_2O
15	----------	H_2, N_2, H_2O
16–20	----------	H_2

[a]Air is assumed to be a mixture of 76.45 wt% N_2 and 23.15 wt% O_2.

Engine component analysis

To solve equations (4) and (6), the respective enthalpies in these equations must be determined. Starting at the engine inlet, the enthalpy terms were evaluated from thermodynamic relationships applied to the specific components in these systems. Pressures at the inlet and outlet of each component were determined from the design point pressures and pressure ratios listed in table I. The equations and procedure applied to the specific components in the engine systems are presented now.

Engine inlet.—Beginning with free-stream conditions at 10 668 m (35 000 ft) altitude and assuming an inlet recovery of 1.0 as stated in table I, the total pressure and total temperature at the inlet (station 1) were computed as follows:

$$P_1 = P_o\left(1 + \frac{\gamma - 1}{2} M^2\right)^{\gamma/(\gamma - 1)} \tag{8}$$

$$T_1 = T_o\left(1 + \frac{\gamma - 1}{2} M^2\right) \tag{9}$$

The enthalpy and entropy of air at station 1 were then obtained from an air properties subroutine formulated from data in reference 7. In functional notation the enthalpy and entropy relationships are as follows:

$$H_1 = f(P_1, T_1) \tag{10}$$

and

$$S_1 = f(P_1, T_1) \tag{11}$$

Turbomachinery.—The fluid conditions at the outlet of a turbomachinery component (such as a compressor, turbine, or pump) were determined as described below. The outlet fluid conditions were computed as follows: For a constant entropy process, the ideal enthalpy at station j ($H_{j,\mathrm{id}}$) is given by

$$H_{j,\mathrm{id}} = f(P_j, S_{j-1}) \tag{12}$$

where the j and $j-1$ are the outlet and inlet flow stations, respectively. For the compressors and pump the actual enthalpy at flow station j is

$$H_j = H_{j-1} + \frac{(H_{j,\mathrm{id}} - H_{j-1})}{\epsilon} \tag{13}$$

And for the turbines, the actual enthalpy at station j is

$$H_j = H_{j-1} + \epsilon(H_{j,\mathrm{id}} - H_{j-1}) \tag{14}$$

Fluid temperatures (corresponding to the actual enthalpies and pressures at station j) were then obtained directly from a subroutine of fluid properties.

Burners—The stoichiometric fuel-to-air mass ratio with hydrogen fuel is 0.029152. To limit the burner outlet temperature to a reasonable preset value, the engine burners must be operated with either rich (ER > 1.0) or

lean (ER < 1.0) fuel mixtures. As stated in the section Description of Topping Cycle Engine, the topping loop burner (B2) operates fuel-rich, and the main engine burner (B1) operates air-rich. The rate of heat release in the respective burners is directly proportional to the rate at which fuel is reacted.

Baseline engine: In the baseline engine (fig. 1), all fuel entering the main burner (B1) is reacted with excess air. The rate of heat release is given by

$$\begin{pmatrix}\text{Rate of heat release}\\ \text{in burner B1}\end{pmatrix} = W_f \Delta H_{comb} \tag{15}$$

The mass ratio of fuel flow to total air flow, W_f/W_a, required to achieve a specified value of burner outlet temperature T_4 is obtained from the heat balance equation; that is,

$$W_f \Delta H_{comb} = (W_a + W_f)(H_4 - H_3) \tag{16}$$

Rearranging equation (16) and solving for the fuel-to-air mass flow ratio gives

$$\frac{W_f}{W_a} = \frac{(H_4 - H_3)}{\Delta H_{comb} - (H_4 - H_3)} \tag{17}$$

The enthalpies of the flow mixtures H_3 and H_4 were calculated from the relationship of equation (7). The value of H_4 in equation (17) is dependent on the temperature and pressure at flow station 4 and also on the fuel-to-air mass flow ratio. Thus, an iterative procedure was used to solve equation (17) for the fuel-to-air mass flow ratio.

Topping cycle engine: In the topping-cycle engine (fig. 2), B2 operates with fuel rich mixtures, and the main burner (B1) operates with lean fuel mixtures. Representing the fuel fraction burned in B2 by X, the rate of heat release in B2 is given by

$$\begin{pmatrix}\text{Rate of heat release}\\ \text{in burner B2}\end{pmatrix} = X(W_f)(\Delta H_{comb}) \tag{18}$$

The combustion products from B2 consist of water vapor, nitrogen, and hydrogen—the unburned fuel. (All oxygen supplied with the bleed air entering B2 is reacted.) The mixed-mean temperature out of B2, (i.e., T_{14} of fig. 2) is specified (see table I) and has a design point value of 1667 K (3000° R). By rearrangement of the heat balance equation for B2, we obtained the following expression for the mass fraction of total fuel flow burned in this burner.

$$X = \frac{\left(1 + \frac{W_f}{W_{bl}}\right)(H_{14} - H_{13})}{\Delta H_{comb}} \tag{19}$$

An iterative procedure was used to solve equation (19). The first step in the procedure was to assume a value for the fuel-to-bleed air mass flow ratio, W_f/W_{bl}. Then, since all oxygen present in the bleed air entering B2 is consumed, we independently computed a value for X from a mass balance around this burner. Using the initial values of W_f/W_{bl} and X, we then calculated the composition of the combustion products leaving B2. The enthalpy of the combustion product mixture, H_{14}, was then calculated from equation (7) for a preselected design point temperature of 1667 K (3000° R). This procedure was repeated, as required, until equation (19) was solved.

The fuel-rich combustion products from B2 are expanded through the topping loop turbine and fed directly into B1. There, the excess fuel in the mixture is combined with the remaining air from the main engine and burned completely. The mass flow rate of fuel entering B1 is equal to $(1 - X)W_f$. The rate of heat release in B1 is given by the following equation:

$$\begin{pmatrix}\text{Rate of heat release}\\ \text{in burner B1}\end{pmatrix} = (1 - X) W_f \Delta H_{comb} \tag{20}$$

The mixed-mean temperature out of B1 (i.e., T_4 of fig. 2) has a specified design point value of 1667 K (3000° R). The total airflow required to achieve this specified temperature is obtained from an energy balance around B1. Thus, the total airflow (including bleed air to the topping loop) is given by

$$W_a = \frac{(1 - X) W_f \Delta H_{comb}}{(H_4 - H_3)} - W_f \tag{21}$$

An iterative procedure was used to solve equation (21). The procedure involved assuming a value of total airflow W_a. This, in turn, fixes the composition of the flow mixture entering and leaving the burner. Then, the respective mixture enthalpies (H_3 and H_4) were computed from the relationship given by equation (7). This procedure was repeated, as required, until a solution of equation (21) was obtained.

(4) ***Heat exchangers.***—The function of the heat exchangers in the topping loop is to reduce the temperature of the airflow entering the compressors. The air temperature at the outlet of each heat exchanger was assumed to have a design point value of 333 K (600° R), and each

heat exchanger was assumed to have a design point pressure ratio of 0.99. (See table I).

With reference to figure 2, the rate of heat transfer from the bleed airflow to the hydrogen flow is given by the following equations: For heat exchanger HX-1

$$Q_{HX-1} = W_{bl}\int_{T_8}^{T_9} C_{p,a}dt \tag{22}$$

And for heat exchanger HX-2

$$Q_{HX-2} = W_{bl}\int_{T_{10}}^{T_{11}} C_{p,a}dt \tag{23}$$

The mixed-mean temperature of the hydrogen flow from HX-1 and HX-2 (i.e., T_{20}) was determined by equating the total heat transfer rate (Q_{HX-1} plus Q_{HX-2}) to the sensible heat gained by the hydrogen flow.

In appendix B a preliminary analysis is presented for the heat exchangers in the topping-cycle engine. In that analysis a particular compact heat exchanger core configuration was considered. Heat exchanger dimensions, surface areas, and weights were estimated for a reference topping-cycle engine system which produces a net shaft power of 7460 kW (10 000 hp).

WEIGHT ANALYSIS

Engine system performance and weight are key factors to consider in the comparison of aircraft propulsion systems. But some of the schemes proposed to improve aircraft engine system performance also result in increases in the system weight and complexity. In view of this an engine system weight study was planned as a part of the overall topping-cycle engine system analysis. The procedure used in this weight study is described below.

A digital computer program, WATE-2 (ref. 9), was used to estimate the weights of both the baseline and topping-cycle engines. To provide a common basis by which these engine weights could be compared, a fixed shaft power output was assumed for each engine system.

WATE-2 is designed to function in conjunction with a specific engine cycle analysis program, known as the NNEP (ref. 7). As a prerequisite to operating WATE-2, a digital simulation must be made for each engine system using the NNEP. Input to the NNEP includes engine thermodynamic data and component data along with logic and control data which describe the order, function, and arrangement of components in the engine system.

The thermodynamic output from the NNEP (which includes temperatures, pressures, flow rates, rotor speeds, shaft powers, etc.) is fed directly into WATE-2. There, weights and dimensions are computed for each of the major components in the engine system. The total engine system weight is then determined by summing the weights of the components along with the calculated weights of structural elements (such as frames, cases, and support hardware).

A separate analysis was made to estimate the weights and dimensions of HX-1 and HX-2 in the topping-cycle engine. This was necessary because the heat exchanger analysis subprogram in WATE-2 is limited to compact heat exchangers in which both working fluids are air. The details of the heat exchanger analysis are presented in appendix B.

In this section we have given a brief description of the procedure used to estimate engine system weights. The accuracy of engine weight estimates from WATE-2 (as stated in ref. 9) is generally ±10 percent. Results of the weight calculations for the baseline and topping-cycle engines are presented and compared in the Results section of this paper.

Results

THERMODYNAMIC PERFORMANCE

In this section the thermodynamic performance of the topping-cycle engine is presented and compared with that of the baseline turboshaft engine which operates under the same cycle conditions. The engine system component characteristics and cycle conditions (design operating conditions) used in this study were introduced in the Thermodynamic Analysis section of this report.

Figure 4 depicts the performance of the topping-cycle engine and the baseline engine for the design operating conditions given in table I. As illustrated in figure 4, the topping-cycle engine performance is significantly better than the baseline engine. At the design conditions given in table I, the thermal efficiency and brake specific fuel consumption of the topping-cycle engine are about 12 percent better than that of the baseline engine.

Several of the design parameters in table I were varied individually for the purpose of examining the topping-cycle engine performance at other cycle conditions. The effects of these individual parametric changes on engine system performance are presented in the following paragraphs.

Effect of Compressor Pressure Ratio

Figure 5 shows the thermal efficiency and bsfc for the baseline and topping-cycle engines against the pressure

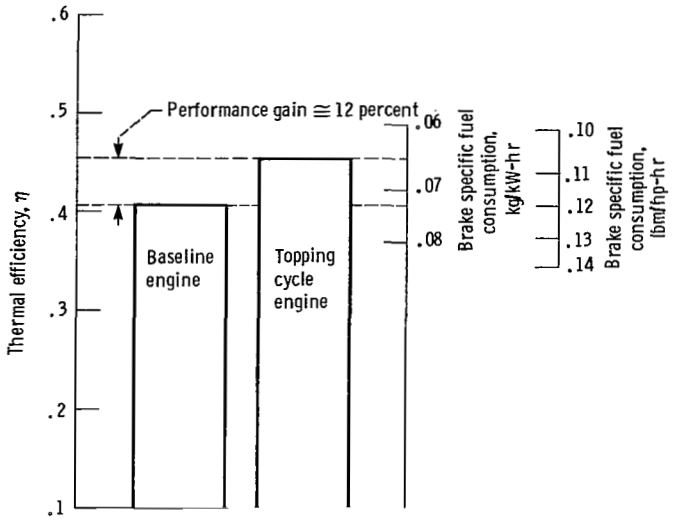

Figure 4. – Comparison of baseline engine and topping-cycle engine performance at design point operating conditions. Altitude, 10 668 m (35 000 ft); Mach 0.8.

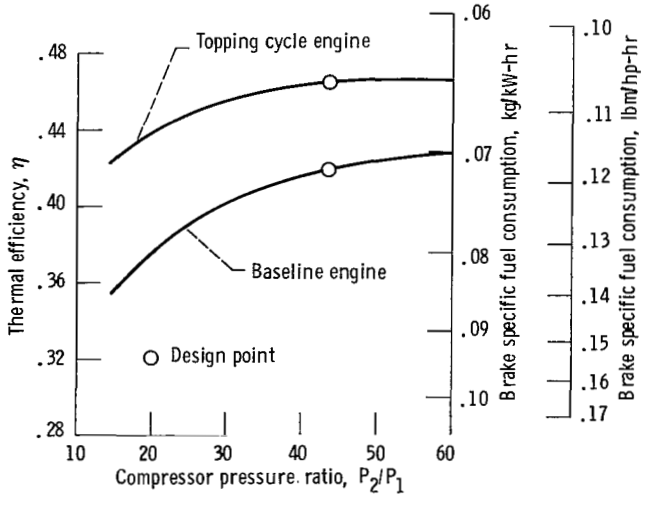

Figure 5. – Thermal efficiency and brake specific fuel consumption as functions of compressor pressure ratios of baseline and topping-cycle engines. Burner temperature, 1667 K (3000° R); altitude, 10 668 m (35 000 ft); Mach 0.80.

ratio of the main compressor (C1). Data in this figure were computed based on a constant design point burner outlet temperature of 1667 K (3000° R). Bleed air pressure to the topping loop was also assumed constant at the design value of 5.59×10^5 N/m^2 (81 psia). As shown in figure 5, the topping cycle engine has a significant performance advantage over the baseline engine throughout the range of compressor pressure ratios shown. The relative difference in the curves of figure 5 ranges from about 12 percent at the design point pressure ratio ($PR = 43.5$) to about 20 percentage points at a pressure ratio of 15.0.

Effect of Burner Temperature

The design point value of burner temperature (table I) was assumed to be 1667 K (3000° R). Cycle calculations were made at other values of burner temperature for the purpose of determining the effect on engine performance. The baseline engine thermal efficiency and bsfc are presented in figure 6 against main compressor (C1) pressure ratio with burner temperature as a parameter. The trends shown in this figure are typical of a conventional turboshaft engine; that is, cycle performance improves with increasing burner temperature, and the optimum or near-optimum compressor pressure ratio (as shown by the dashed line) increases with burner temperature.

A similar plot showing the effect of burner temperature on the topping-cycle engine performance is depicted in figure 7. In the topping-cycle engine both burners are assumed to operate at the same constant temperature. A comparison of data in figures 6 and 7 indicates that the topping-cycle engine performance is significantly better than the baseline engine performance at all values of burner temperature. With the main compressor operating at the design point pressure ratio of 43.5, the relative difference in performance of these engines is approximately 12 percent for all constant values of burner temperature. At lower values of main compressor pressure ratio (e.g., near 15), the relative difference in performance of these engines is on the order of 15 to 20 percent for the range of operating temperatures shown in figures 6 and 7. Figure 7 also indicates that at the burner design point temperature of 1667 K (3000° R), the optimum pressure ratio of the topping-cycle engine is

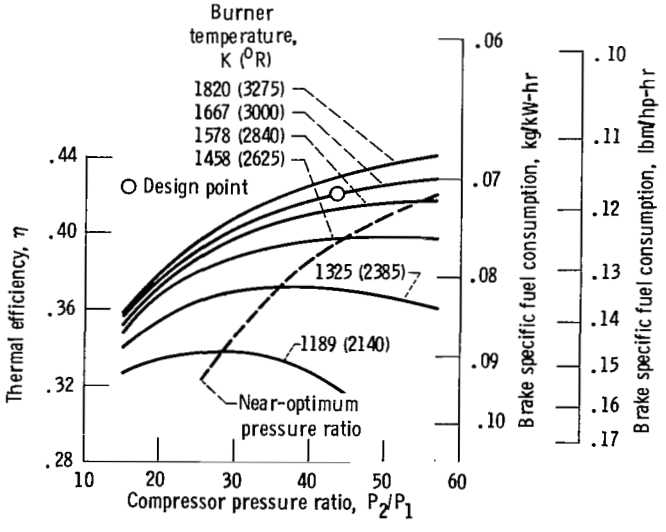

Figure 6. – Baseline engine thermal efficiency and brake specific fuel consumption as functions of compressor pressure ratio. Altitude, 10 668 m (35 000 ft); Mach 0.8.

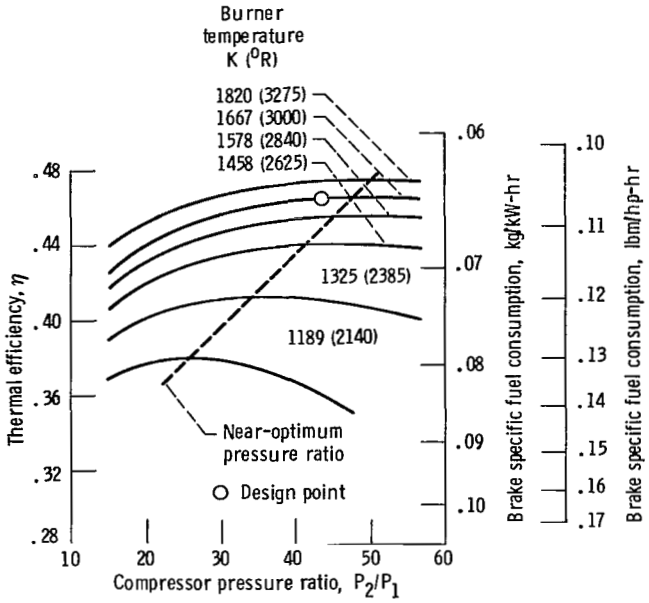

Figure 7. – Topping-cycle engine thermal efficiency and brake specific fuel consumption as functions of compressor pressure ratio. Altitude, 10 668 m (35 000 ft); Mach 0.8.

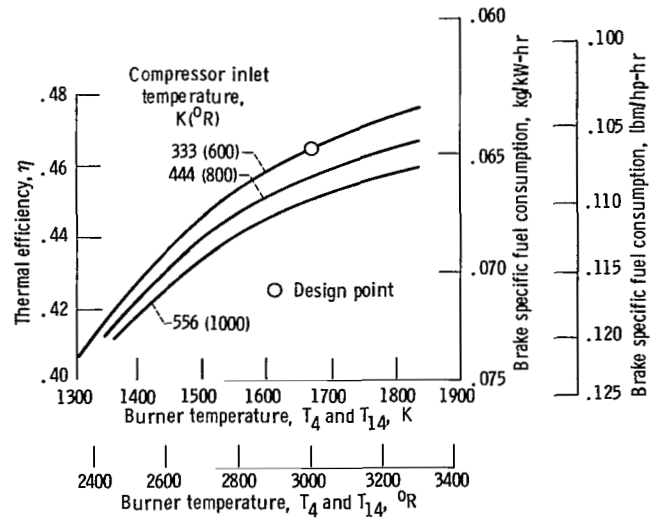

Figure 8. – Topping-cycle engine thermal efficiency and brake specific fuel consumption as function of burner temperature with topping-loop compressor inlet temperature as parameter. Altitude, 10 668 m (35 000 ft); Mach 0.8.

near the selected design point pressure ratio of 43.5, as given in table I.

Effect of Precooling Compressor Air in Topping Loop

Precooling of the bleed air in the topping loop is accomplished with hydrogen-to-air heat exchangers as shown in figure 2. As stated in the Description of Topping Cycle Engine section, the purpose of precooling is to reduce the work requirements of compressors C2 and C3. The effect of precooling is shown in figure 8 where the thermal efficiency and bsfc of the topping-cycle engine are presented against burner temperature for different values of compressor inlet temperature. As shown, the relative performance of the topping-cycle engine increases with the level of precooling. At a burner temperature of 1667 K (3000° R), that is, the design value, the relative performance gain from precooling is on the order of 1 percent for a change in compressor air inlet temperature of 55 K (100° R).

From the data in figure 8 it would appear that further improvements in performance could be obtained by precooling the bleed air to a temperature below the design point value of 333 K (600° R). However, there is a practical limit to the amount of precooling. At the design point operating conditions, the heat transfer rates in both of the heat exchangers are approximately equal, and the design point effectiveness of each heat exchanger is in the neighborhood of 65 percent. Additional precooling would require a higher value of heat exchanger effectiveness which, in turn, would call for physically larger heat exchangers. Another point is that a small amount of moisture (water vapor) is normally present in the ingested airflow, even at high altitudes. The likelihood of the entrained moisture condensing and freezing on the air-side surfaces of the heat exchangers could increase with the amount of precooling. To preclude this possibility and also to have the heat exchangers operate with reasonable effectiveness, a minimum bleed air temperature of 333 K (600° R) was assumed as a reasonable condition for this study.

Effect of Heat Exchanger Pressure Losses

At the design point the pressure losses in the heat exchangers were assumed to be 1 percent of the inlet pressure. Thus, the design value for each of the individual ratios of pressure loss to inlet pressure (i.e., $(P_8-P_9)/P_8$, $(P_{10}-P_{11})/P_{10}$, $(P_{18}-P_{19})/P_{18}$, and $(P_{16}-P_{17})/P_{16}$) was assumed equal to 0.01.

The sensitivity of the topping-cycle engine performance to heat exchanger pressure losses is shown in figure 9. At the design point burner temperature of 1667 K (3000° R), the data in figure 9 indicate that the relative change in performance is about 1 percent for each 5 percent change in heat exchanger pressure ratio (or 5 counts of pressure drop).

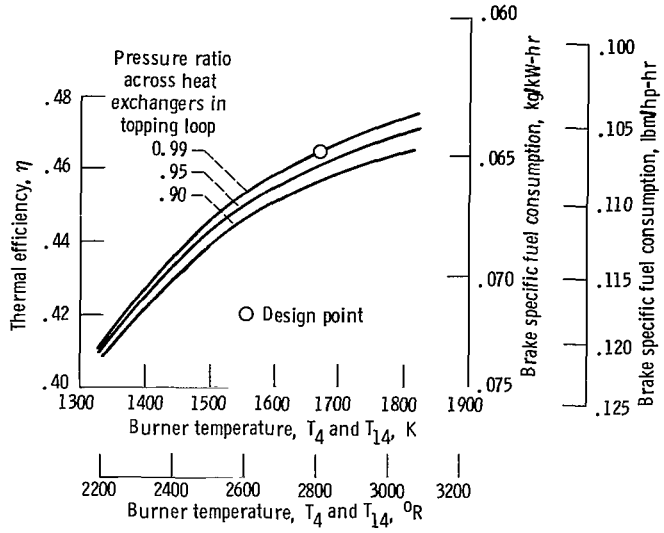

Figure 9. – Topping-cycle engine thermal efficiency and brake specific fuel consumption as function of burner temperature with topping-loop heat exchanger pressure ratio as parameter. Altitude, 10 668 m (35 000 ft); Mach 0.8.

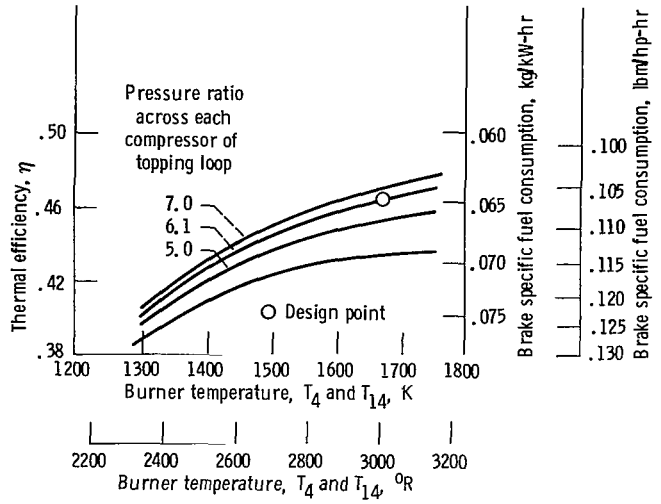

Figure 10. – Topping-cycle engine thermal efficiency and brake specific fuel consumption as function of burner temperature with pressure ratio across each compressor in topping loop as parameter. Altitude, 10 668 m (35 000 ft); Mach 0.8.

Effect of Compressor Pressure Ratio in Topping Loop

The effect of the topping loop compressor pressure ratio on engine performance is shown in figure 10. As indicated in this figure, cycle performance improves with increases in the topping loop compressor pressure ratio. There is, however, a practical upper limit to the compressor pressure ratio. At the design point the pressure ratio across each compressor in the topping loop was equal to 6.10. (See table I.) This pressure ratio was chosen as a design value so as to limit the absolute pressure in the topping loop to a value of about 2.06×10^7 Pa (3000 psia).

It appears that additional improvements in performance may be realized by increasing the compressor pressure ratio above the design point value of 6.10 (fig. 10). However, a relatively small increase in the compressor pressure ratio results in a large change in absolute pressure in the topping loop. For example, increasing the pressure ratio of each compressor from 6.10 to 7.0 results in a pressure increase of about 6.87×10^6 Pa (1000 psia) in the topping loop.

Effect of Hydrogen Turbopump Efficiency

In this study the hydrogen turbopump was assumed to have an overall efficiency of 60 percent. At the design operating conditions, hydrogen enters the turbopump as a saturated liquid at 1 atm pressure. The hydrogen pressure is then boosted by the turbopump to a level near 217 atm. Since the specific volume of hydrogen is relatively small, the pumping power per unit hydrogen mass flow is likewise small, even for the large change in pressure.

At the design operating conditions the power input to the hydrogen turbopump is less than 1 percent of the topping-cycle engine shaft power output. And because of the low input power requirements of the turbopump, the performance of this engine is relatively insensitive to the turbopump efficiency.

TOPPING-CYCLE ENGINE PERFORMANCE

The foregoing discussion has shown that the efficiency and/or bsfc of the topping-cycle engine is about 12 percent better than that of a baseline turboshaft engine operating at the same cycle conditions. Before proceeding, it is important to note that a significant fraction of the net shaft power output of the topping-cycle engine is generated by the auxiliary topping loop. At the design operating conditions the topping loop delivers about 22 percent of the total shaft power output of this engine system. Thus, the efficiency with which this loop functions can have a significant effect on the overall performance of the topping-cycle engine. In this section we shall consider the individual factors which contribute to the overall performance gain associated with this engine system.

Precooling of Compressor Airflow in Topping Loop

The precooling of airflow upstream of each compressor in the topping loop reduces the work input to the compressors. Along with the compressor air precooling, the fuel is also preheated somewhat in this process. The combined effect of precooling the compressor airflow and preheating the fuel results in a cycle performance improvement of about 1 percent per 55 K (100° R) change in the compressor inlet airflow temperature.

Utilization of Fuel as a Working Fluid

A significant net gain is realized from the use of fuel as a working fluid in this cycle. The heated, unburned hydrogen fuel passing through the topping loop turbine generates a large fraction of the topping loop turbine power output. At the design conditions only about 6 percent of the mass flow through the topping loop turbine is unburned hydrogen fuel. But, because hydrogen has a high specific heat (nearly 15 times that of air), the turbine work produced by the unburned hydrogen amounts to about 48 percent of the total work produced by this turbine. On the other hand, the pumping power required to boost the pressure of the cryogenic fuel (which is stored as a saturated liquid) is relatively small. At design conditions only about 2.5 percent of the power output of the topping loop turbine is used to drive the turbopump. Thus, in this cycle the topping loop operates very efficiently. In terms of the overall performance gain associated with the topping-cycle engine, approximately 80 percent of this gain can be attributed to the efficient use of the fuel also as a working fluid in the topping loop of this engine.

ENGINE SYSTEM WEIGHTS

The results of the weight studies for the baseline engine and topping-cycle engine are described herein. Weight estimates obtained from WATE-2 and presented herein are based on a common shaft power output of 7460 kW (10 000 hp) for each engine system. The procedure used in estimating engine system weights is described in the Weight Analysis section.

Baseline Engine

The calculated weights for the baseline engine are summarized in table III. The baseline engine is actually a two-spool engine. And the turbomachinery weights listed in table III include the individual high and low spool components. (The requirement of two spools is dictated by the relatively large overall pressure ratio of the engine.)

The compressor and turbine weights listed in table III include the weights of the disk, blades, stators, connecting hardware, frame, and case. But, as indicated in table III, inlet and exhaust system weights are not included in the total engine system weight. The total weight of the baseline engine as estimated from WATE-2 is shown in table III to be 386 kg (850 lbm).

TABLE III. – COMPONENT WEIGHTS AND ENGINE SYSTEM WEIGHT FOR 7450-kW (10 000 hp) BASELINE TURBOSHAFT ENGINE

Component	Weight	
	kg	lbm
Compressor C1:		
LPC	157	347
HPC	46	101
Burner B1	37	81
Turbine T1:		
HPT	31	69
LPT	57	125
Shafting	13	28
Controls and accessories	45	99
Total engine	386	850

Topping-Cycle Engine

The calculated weights for the topping-cycle engine are listed in table IV. The main, gas-turbine engine of this system also has two rotating spools.

The compressor and turbine weights in table IV include the same hardware items as described for the baseline engine. Gearbox weights and inlet and exhaust system weights are not included in the total topping-cycle engine weight.

Because of the relatively low mass flow rates in the topping loop, the compressors in this loop (C2 and C3) were assumed to be centrifugal machines. The total weight of the topping-cycle engine as estimated from WATE-2 (and listed in table IV) is 392 kg (865 lbm). A comparison of the computed weights for the baseline and topping-cycle engines indicates that they are nearly the same.

TABLE IV. – COMPONENT WEIGHTS AND ENGINE SYSTEM WEIGHT FOR 7460 kW (10 000 hp) TOPPING-CYCLE ENGINE

Components	Weight	
	kg	lbm
Main gas turbine engine:		
Compressor C1:		
LPC	123	271
HPC	37	82
Burner B1	28	62
Turbine T1:		
HPT	24	52
LPT	45	100
Shafting	10	22
Controls and accessories	34	75
Main gas turbine engine:		
Topping loop:		
Compressors C2	18	40
Compressors C3	9	20
Burner B2	10	22
Turbine T2	26	57
Heat exchanger HX-1	4	9
Heat exchanger HX-2	9	20
Shafting	5	11
Controls and accessories	10	22
Topping loop	91	201
Total engine	392	865

In comparing these engine weights it is important to note that the specific power of the topping-cycle engine is significantly greater than that of the baseline engine. (Specific power as used here is defined as the ratio of engine shaft power output to total engine airflow.) For a fixed value of shaft power output, the total airflow of the topping-cycle engine was calculated to be about 28 percentage points less than that of the baseline engine. The lower airflow (or higher specific power) results in smaller and lighter-weight engine components. Thus, even though the topping-cycle engine has an auxiliary flow loop that contains additional components, the estimated total weight of this engine system is comparable with that of the baseline turboshaft engine.

Summary of Results

The thermodynamic performance of the topping-cycle engine was analyzed and compared with that of a reference turboshaft engine which operates under the same cycle conditions. For the cycle operating conditions selected, the performance of the topping-cycle engine (i.e., the efficiency and/or bsfc) was determined to be about 12 percent better than that of a reference turboshaft engine.

The improved overall performance of this engine can be attributed to the fact that the auxiliary topping loop is highly efficient. In the topping loop, cryogenic fuel (stored as a saturated liquid) is boosted to a high pressure by a turbopump. Because the fuel has a relatively small specific volume, the power expended in pumping the fuel is also relatively small, even for the large pressure change. The high pressure-low temperature fuel is also used to precool the bleed airflow in this loop before compression. This, in turn, reduces the work required to compress the bleed airflow. Finally, the high pressure fuel is heated and a portion of it is then expanded through an auxiliary power turbine to produce additional shaft power. The combination of these processes results in a significant improvement in the overall performance of the topping-cycle engine.

The results of the weight comparison between the topping-cycle engine and the baseline turboshaft engine indicate that these engines have nearly the same weight. The weight comparison was based on a common shaft power output of 7460 kW (10 000 hp) for each engine.

It is concluded, therefore, that the topping-cycle engine has significantly better thermodynamic performance than that of the baseline turboshaft engine. And the estimated weight of the topping-cycle engine is comparable to that of the baseline turboshaft engine.

National Aeronautics and Space Administration
Lewis Research Center
Cleveland, Ohio, October 7, 1983

Appendix A
Symbols

A_{fin}	fin surface area per unit length of finned tube, m^2/m; ft^2/ft
$A_{f,sh}$	shell flow area per unit shell length, m^2/m; ft^2/ft
$A_{f,tube}$	flow area per tube, m^2; ft^2
A_i	inside surface area per unit length of tube, m^2/m; ft^2/ft
A_o	outside surface area per unit length of tube, m^2/m; ft^2/ft
$A_{o,tot}$	total outside surface area per unit length of tube, m^2/m; ft^2/ft
A_s	surface area of heat exchanger (eq. (B15)), m^2; ft^2
bsfc	brake specific fuel consumption, $kg_{fuel}/kW\text{-}hr$; $lb_{fuel}/hp\text{-}hr$
$C_{p,a}$	specific heat of air at constant pressure, kW-hr/kg-K, Btu/lbm-°R
$C_{p,H}$	specific heat of hydrogen at constant pressure, kW-hr/kg-K; Btu/lbm-°R
D_i and D_{tube}	inside diameter of heat exchanger tube, m; ft
D_o	outside diameter of heat exchanger tube, m; ft
D_{sh}	hydraulic diameter on shell side of heat exchanger, m; ft
E	heat exchanger effectiveness
$\mathcal{E}$	turbomachine efficiency
f_{sh}	friction factor on shell side of heat exchanger
f_{tube}	friction factor inside tubes of heat exchanger
G_{sh}	mass velocity of air in heat exchanger shell, $kg/m^2\text{-}hr$; $lbm/ft^2\text{-}hr$
G_{tube}	mass velocity of hydrogen in heat exchanger tubes, $kg/m^2\text{-}hr$; $lbm/ft^2\text{-}hr$
g_c	conversion factor, 1.296×10^7 kg-m/N-hr^2; 4.17×10^8 lbm-ft/lbf-hr^2
H	enthalpy, kW-hr/kg; Btu/lbm
ΔH_{comb}	heat of combustion of hydrogen fuel, 33.251 kW-hr/kg; 51 500 Btu/lbm
H_i	enthalpy of component i in gas mixture, kW-hr/kg; Btu/lbm
H_{mix}	enthalpy of gas mixture (eq. (7)), kW-hr/kg; Btu/lbm
h_{sh}	heat transfer coefficient on shell side of heat exchanger, $kW/m^2\text{-}K$; $Btu/hr\text{-}ft^2\text{-}°R$
h_{tube}	heat transfer coefficient inside tubes of heat exchanger, $kW/m^2\text{-}K$; $Btu/hr\text{-}ft^2\text{-}°R$
h_t	active height of tubes in heat exchanger, m; ft
K	conversion factor (eqs. (4) and (6)), 1.0; 3.927×10^{-4} hp-hr/Btu
k_{Al}	thermal conductivity of aluminum, kW/m-K; Btu/hr-ft-°R
L_{tube}	total length of tube passage in heat exchanger, m; ft
M	Mach number
P	total pressure, Pa; psia
ΔP_{sh}	pressure drop on shell side of heat exchanger, Pa; psi
ΔP_{tube}	pressure drop on tube side of heat exchanger, Pa; psi
Pr_a	Prandtl number for air
Pr_h	Prandtl number for hydrogen
$Q_{HX\text{-}1}$	heat transfer rate in heat exchanger HX-1, kW; Btu/hr
$Q_{HX\text{-}2}$	heat transfer rate in heat exchanger HX-2, kW; Btu/hr
Re_{sh}	Reynolds number on shell side of heat exchanger
Re_{tube}	Reynolds number on tube side of heat exchanger
S	entropy, kW-hr/K; Btu/°R
SP	shaft power output of engine, kW; hp
T	temperature, K; °R
ΔT_{lm}	log-mean temperature difference in heat exchanger, K; °R
t_{header}	thickness of heat exchanger inlet and outlet headers, m; ft
t_{sh}	thickness of heat exchanger shell, m; ft
U	overall coefficient of heat transfer (eq. (B13)), $kW/m^2\text{-}K$; $Btu/hr\text{-}ft^2\text{-}°R$
W_a	airflow rate, kg/hr; lbm/hr
W_{bl}	bleed airflow rate, kg/hr; lbm/hr
W_f	fuel flow rate, kg/hr; lbm/hr
W_i	flow rate of component *i* in flow mixture (eq. (7)), kg/hr; lbm/hr
γ	specific heat ratio for air
η	thermal efficiency
η_{fin}	heat transfer efficiency of fins

η_{os}	overall heat transfer efficiency of outer finned tubes surface
μ_a	viscosity of air, kg/m-hr; lbm/ft-hr
μ_H	viscosity of hydrogen, kg/m-hr; lbm/ft-hr
ρ_a	density of air, kg/m^3; lbm/ft^3
ρ_H	density of hydrogen, kg/m^3; lbm/ft^3
X	fraction of total fuel burned in burner B2

Subscripts:

0	refers to atmospheric free-stream conditions
1-19	flow station designations (see figs. 1 and 2)
id	ideal
eq	equivalent (see eq. (B19))
j	flow station j
j-1	flow station j-1

Appendix B
Heat Exchanger Analysis

A preliminary analysis is presented herein for the heat exchangers in the topping cycle engine. Starting with a particular compact heat exchanger configuration, estimates were made of the areas, dimensions and weights of the topping loop heat exchangers. A reference topping cycle engine with a shaft power output of 7460 kW (10 000 hp) was used as a basis for the calculations.

Several compact heat exchanger configurations could be considered for this application. One configuration which appeared reasonable (from assessments of the fluid flow rates, pressures and temperatures) is a crossflow configuration with multipass finned circular tubes, identified as "surface CF-8.72" by Kays and London (ref. 10). In this arrangement the hydrogen flows inside the tubes, and the air flows normal to the finned tubes in a crossflow direction (fig. 11).

The dimensional constants for this finned tube configuration (surface CF-8.72) are as follows:

Tube outside diameter, cm (in.)	0.965 (0.38)
Fin outside diameter, cm (in.)	2.34 (0.92)
Fin thickness, cm (in.)	0.046 (0.018)
Fin spacing, cm^{-1} (in^{-1})	3.43 (8.72)
Tube spacing (lateral), P, cm (in.)	2.48 (0.975)
Tube row spacing, S, cm (in.)	2.03 (0.155)
Hydraulic diameter (air side), cm (in.)	0.393 (0.155)
Percent of free flow area	52.4
Ratio of surface area to volume	163.0

For the low temperature conditions involved in this application, the heat exchangers may be constructed of aluminum. The tube wall thickness thus required for an internal pressure of 20.68×10^6 Pa (3000 psi) and an allowable stress of 1.034×10^8 Pa (15 000 psi) is approximately 0.089 cm (0.035 in). The surface areas and flow areas associated with this finned tube configuration are summarized in table V.

The heat loads and fluid temperatures in both topping loop heat exchangers (HX-1 and HX-2) are nearly identical. The only condition that is significantly different is the pressure level on the shell side (airflow side) of the heat exchangers. The pressure level there is an important consideration in the mechanical design of the heat exchanger containment shell. However, for the thermal analysis, the effect of pressure level on the shell side is relatively insignificant. Because of the close similarity in the operating conditions of both heat exchangers, a single thermal analysis based on the conditions of HX-1 should be applicable also to HX-2.

THERMAL ANALYSIS

The inlet and outlet fluid temperatures of heat exchanger HX-1 are

	Temperature, K (°R)
Hydrogen inlet, T_{18}	45.7 (82.3)
Hydrogen outlet, T_{19}	397.2 (715.0)
Air inlet, T_8	578.9 (1042.0)
Air outlet, T_9	333.3 (600.0)

Table VI contains a listing of some of the physical properties of hydrogen and air used in this analysis. The values listed were obtained from references 11 and 12 and are based on the respective fluid mean temperatures inside HX-1.

For the reference topping cycle engine with a shaft power output (SP) of 7460 kW (10 000 hp) and

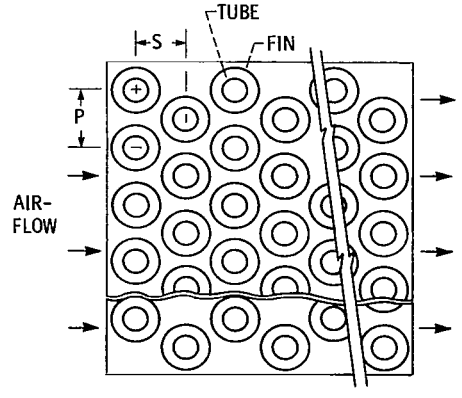

Figure 11. – Tube pattern and dimensions for crossflow heat exchanger with multipass, finned, circular tubes (surface CF-8.72).

TABLE V. – SURFACE AREAS AND FLOW AREAS OF FINNED TUBE CONFIGURATION CF-8.72

Surface areas per unit length of finned tube, m^2/m (ft^2/ft):	
Tube inside surface area, A_i	0.0247 (0.0812)
Tube outside surface area, A_o	0.0256 (0.0839)
Fin surface area, A_{fin}	0.2558 (0.8391)
Total outside surface area, $A_{o,tot}$	0.2814 (0.9230)
Surface area ratios:	
Fin surface area/total outside surface area, $A_{fin}/A_{o,tot}$	0.910
Inside surface area/total outside surface area, $A_i/A_{o,tot}$	0.088
Flow areas:	
Tube flow area per tube, $A_{f,tube}$, m^2 (ft^2)	48.7×10^{-6} (5.24×10^{-4})
Shell flow area per unit length, $A_{f,sh}$, m^2/m (ft^2/ft)	0.0130 (0.0426)

TABLE VI. – PHYSICAL PROPERTIES OF HYDROGEN AND AIR USED IN ANALYSIS OF HEAT EXCHANGER HX-1

	Hydrogen	Air
Specific heat, C_p, kW-hr/kg-K (Btu/lbm-°R)	4.162×10^{-3} (3.58)	2.883×10^{-4} (0.248)
Viscosity, μ, kg/m-hr (lbm/ft-hr)	2.813×10^{-2} (1.89×10^{-2})	10^{-2} (6.084×10^{-2})
Prandtl number, Pr	0.73	0.683
Density, ρ, kg/m^3 (lbm/ft^3)	19.286 (1.204)	4.240 (0.265)

$bsfc = 0.0647$ kg/kW-hr (0.1064 lbm/hp-hr), the total fuel flow rate is given by

$$W_f = SP \times bsfc = 482.5 \text{ kg/hr}$$

$$= 1063.8 \text{ lbm/hr} \quad \text{(B1)}$$

Assuming that one-half of the total fuel flow passes through each exchanger, the rate of heat transfer in HX-1 is

$$Q_{\text{HX-1}} = \frac{W_f}{2} C_{p,H}(T_{19} - T_{18}) = 352.94 \text{ kW}$$

$$= 1.205 \times 10^6 \text{ Btu/hr} \quad \text{(B2)}$$

And the corresponding flow rate of bleed air is

$$W_{\text{bl}} = \frac{Q_{\text{HX-1}}}{C_{p,a}(T_8 - T_9)} = 4985.7 \text{ kg/hr}$$

$$= 10\,993 \text{ lbm/hr} \quad \text{(B3)}$$

The effectiveness of HX-1 is given by the equation

$$E = \frac{Q_{\text{HX-1}}}{W_f C_{p,H}(T_8 - T_9)} = 0.659 \quad \text{(B4)}$$

For the purpose of estimating the heat transfer and flow characteristics of the heat exchanger, we shall assume the following:

(1) The heat exchanger has eight finned tubes in each tube layer

(2) Each finned tube has an active height h_t of 0.2032 m (8 in.)

(3) The tubes of each layer are connected to the tubes of adjacent layers by return bends to form a multipass tube flow arrangement.

Estimate of Tube Side Friction Factor and Heat Transfer Coefficient

With eight tubes per layer, the mass velocity of hydrogen flow inside the tubes is given by

$$G_{\text{tube}} = \frac{W_f/2}{8A_{f,\text{tube}}} = 6.193 \times 10^5 \text{ kg/m}^2\text{-hr}$$

$$= 1.269 \times 10^5 \text{ lbm/ft}^2\text{-hr} \quad \text{(B5)}$$

And the Reynolds number inside the tubes is

$$\text{Re}_{\text{tube}} = \frac{G_{\text{tube}} D_{\text{tube}}}{\mu_H} = 1.734 \times 10^5 \quad \text{(B6)}$$

The friction factor for flow inside the tubes is given by the expression (ref. 13)

$$f_{\text{tube}} = 0.046 (\text{Re}_{\text{tube}})^{-0.20} = 0.00412 \quad \text{(B7)}$$

From the Reynolds analogy, as modified by Colburn (ref. 14), the heat transfer coefficient for flow inside the tubes is

$$h_{\text{tube}} = \frac{G_{\text{tube}} C_{p,H} f_{\text{tube}}}{2(\text{Pr}_H)^{2/3}} = 6.552 \text{ kW/m}^2\text{-K}$$

$$= 1176.1 \text{ Btu/hr-ft}^2\text{-°R} \quad \text{(B8)}$$

Estimate of Shell Side Friction Factor and Heat Transfer Coefficient

On the shell side of the heat exchanger, the mass velocity of airflow through the layer of eight tubes is computed as follows:

$$G_{\text{sh}} = \frac{W_{\text{bl}}}{8A_{f,\text{sh}}} = 2.362 \times 10^5 \text{ kg/m}^2\text{-hr}$$

$$= 4.84 \times 10^4 \text{ lbm/ft}^2\text{-hr} \quad \text{(B9)}$$

and Reynolds number on the shell side is

$$\text{Re}_{\text{shell}} = \frac{G_{sh} D_{\text{sh}}}{\mu_a} = 10\,279 \quad \text{(B10)}$$

In equation (B10), D_{sh} is the hydraulic diameter on the air flow side (shell side) of the heat exchanger. (See fig. 11 for numerical value of D_{sh}.) The friction factor on the shell side is obtained directly from the data given by Kays and London (ref. 10). For surface configuration CF-8.72, we have

$$f_{sh} = 0.030$$

Based on the Reynolds number computed in equation (B10), the shell side heat transfer coefficient (with some extrapolation of the ref. 10 data) is given by

$$h_{sh} = \frac{0.0056\, G_{sh} C_{p,a}}{(\mathrm{Pr}_a)^{2/3}} = 0.503 \text{ kW/m}^2\text{-K}$$

$$= 89.72 \text{ Btu/hr-ft}^2\text{-°R} \qquad \text{(B11)}$$

Estimate of Overall Heat Transfer Coefficient and Surface Area Requirement

The efficiency of the finned tubes in transferring heat is a function of the tube and fin dimensions, the thermal conductivity of the fins, and the shell side heat transfer coefficient. For surface configuration CF-8.72 with aluminum fins, the fin efficiency μ_{fin} is estimated from data in reference 10 to be 0.78.

The overall efficiency of the outer surface is obtained by combining the unfinned portion of the tube surface at 100 percent efficiency with the surface area of the fins at efficiency η_{fin}. In surface configuration CF-8.72, the ratio of fin surface area to total outer surface area (from table V) is equal to 0.91. And the overall efficiency of the outer surface, η_{os} is computed as follows:

$$\eta_{os} = \frac{1 - A_{fin}}{A_{o,tot}} + \left(\frac{A_{fin}}{A_{o,tot}}\right)\eta_{fin} \qquad \text{(B12)}$$

Inserting the numerical values into equation (B12) gives

$$\eta_{os} = 0.80$$

The overall heat transfer coefficient (based on the outer surface area of the finned tubes) is given by the following expression:

$$u = \frac{1}{\frac{D_o}{D_i h_{tube}} + \frac{D_o \ln(D_o/D_i)}{k_{al}} + \frac{1}{\eta_{os} h_{shell}}} \qquad \text{(B13)}$$

Inserting the appropriate numerical values into equation (B13), we have

$$U = 0.3775 \text{ kW/m}^2\text{-hr}$$

$$= 66.527 \text{ Btu/hr-ft}^2\text{-°R}$$

It will be shown later in the analysis that several tube passes are needed in this crossflow heat exchanger to satisfy the heat transfer area requirement. Data from reference 15 indicates that with three or more tube passes, the true mean temperature difference of a crossflow heat exchanger is essentially equal to the log-mean temperature difference of a counterflow heat exchanger. Therefore, for this crossflow heat exchanger, we can use the log-mean temperature difference as described by the following equation:

$$\Delta T_{lM} = \frac{(T_8 - T_{19}) - (T_9 - T_{18})}{ln \frac{(T_8 - T_{19})}{(T_9 - T_{18})}} \qquad \text{(B14)}$$

Inserting the temperatures into equation (B14), we have

$$\Delta T_{lM} = 230.6 \text{ K} = 415.1° \text{ R}$$

And the required surface area of the crossflow heat exchanger is given by the equation

$$A_s = \frac{Q_{HX-1}}{U\, \Delta T_{lM}} = 4.05 \text{ m}^2 = 43.638 \text{ ft}^2 \qquad \text{(B15)}$$

With eight finned tubes in each layer, the number of tube layers required is

$$\text{Layers required} = \frac{A_s}{8 A_{o,tot} h_t} = 8.865 \qquad \text{(B16)}$$

Therefore, we shall assume that the heat exchanger has nine tube layers. And the dimensions and volume of the heat exchanger core are as follows:

Depth of heat exchanger core, $8S + D_{fin}$, cm (in.)	18.59 (7.32)
Width of heat exchanger core, 8.5p, cm (in.)	21.05 (8.29)
Height of heat exchanger core, cm (in.)	20.32 (8.00)
Volume of heat exchanger core, m^3 (ft^3)	0.0080 (0.281)

Figure 12 is a sketch of the finned tube core for HX-1 and HX-2.

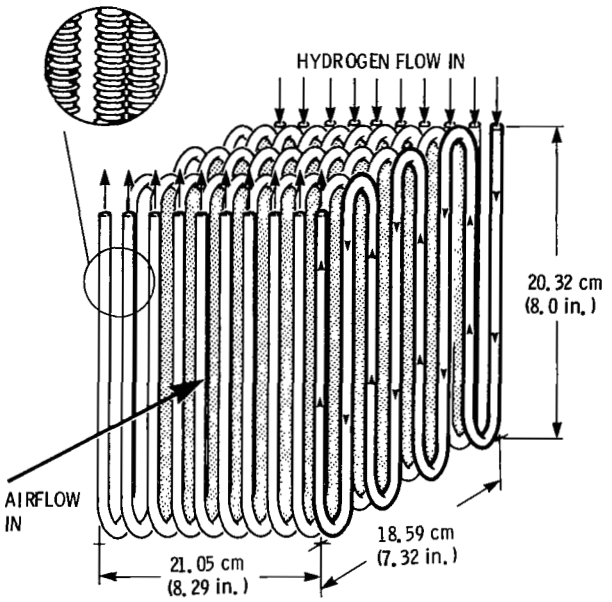

Figure 12. – Finned tube core for heat exchangers HX-1 and -2.

HEAT EXCHANGER WEIGHT

The total weight of the heat exchanger includes the weight of the finned tubes, the outer shell, and the inlet and outlet headers.

Finned Tubes

The weight breakdown of the aluminum finned tube flow passages is summarized below:

Tube weight, including return bends, kg (lbm) 0.964 (2.136)
Total tube length, m (ft) 14.638 (48.0)
Fin weight (total number of fins = 5023), kg (lbm).....2.210 (4.875)
Total weight of finned tubes, kg (lbm) 3.174 (7.011)

Outer Shell

For this preliminary analysis, we shall consider the shell to be cylindrical with an inside diameter of 0.293 m (11.52 in.). (This inside diameter is the minimum diameter needed to contain the core of finned tubes.) Assuming the allowable stress for aluminum to be 6.89×10^7 Pa (10 000 psi), the required shell thickness, t_{sh}, is given by

$$t_{sh} = \frac{\text{(internal pressure)(shell projected area)}}{\text{2(shell length)(allowable stress)}} \qquad \text{(B17)}$$

(The allowable stress for the shell is less than that used for the tubes because of the higher average temperature of the shell.)

For HX-1, with an internal pressure of 5.52×10^5 Pa (80 psi), the computed values of shell thickness and shell weight are

Shell thickness for HX-1, cm (in.) 0.117 (0.046)
Shell weight for HX-1, kg (lbm) 0.5423 (1.197)

And for HX-2, with an internal pressure of 3.31×10^6 Pa (480 psi), the computed values of shell thickness and shell weight are

Shell thickness for HX-2, cm (in.) 0.704 (0.277)
Shell weight for HX-2, kg (lbm).....3.254 (7.182)

Inlet and Outlet Headers

For simplicity, we shall consider the inlet and outlet headers to be hemispherical shells. Again, assuming an allowable stress for aluminum of 6.89×10^7 Pa (10 000 psi), the header thickness required to withstand the internal pressure is given by the relation

$$t_{header} = \frac{\text{(internal pressure)(projected area of header)}}{\text{(mean perimeter of hemispherical shell)(allowable stress)}} \qquad \text{(B18)}$$

For HX-1 the computed values of header thickness and header weight are

Header thickness for HX-1, cm (in.).....0.0589 (0.02318)
Header weight for HX-1 (2 headers), kg (lbm) 0.4357 (0.9605)

And the computed values of header thickness and header weight for HX-2 are

Header thickness for HX-2, cm (in.) 0.3534 (0.1391)
Header weight for HX-2 (2 headers), kg (lbm) 2.614 (5.763)

A summary of the computed weights for HX-1 and HX-2 is presented in table VII.

TABLE VII. – SUMMARY OF COMPUTED WEIGHTS FOR HEAT EXCHANGERS

Component	Heat exchanger	
	HX-1	HX-2
	Weight, kg (lbm)	
Finned tube core	3.174 (7.001)	3.174 (7.001)
Cylindrical shell	.542 (1.197)	3.254 (7.182)
Inlet and outlet headers	.436 (.961)	2.614 (5.763)
Total weight per heat exchanger	4.152 (9.159)	9.042 (19.946)
Total weight of HX-1 and HX-2	13.194 kg (29.105 lbm)	

ESTIMATE OF PRESSURE LOSSES

The fluid pressure drops due to friction were determined as follows: For the hydrogen flow inside the tubes the pressure drop due to friction is given by

$$\Delta P_{tube} = \frac{(G_{tube})^2}{2gC_{p,H}} 4f_{tube}\left(\frac{L_{tube}}{D_{tube}}\right)_{eq} \quad \text{(B19)}$$

The equivalent length-to-diameter ratio in equation (B19) includes the physical length-to-diameter ratio of the flow passages and the effective length-to-diameter ratio of the tube return bends. The effective length-to-diameter ratio for each close pattern return bend is equal to 50 (ref. 10). So, the equivalent length-to-diameter ratio of nine tube passes with nine close pattern return bends was determined from the following expression:

$$\left(\frac{L_{tube}}{D_{tube}}\right)_{eq} = \frac{\text{(number of tube layers)(tube length per layer)}}{D_{tube}} + \text{(number of return bends)(effective } L/D \text{ per bend)} \quad \text{(B20)}$$

Inserting the appropriate values into equation (B20) gives

$$\left(\frac{L_{tube}}{D_{tube}}\right)_{eq} = 9(25.81) + 9(50) = 682.3$$

And from equation (B19), the hydrogen pressure drop inside the finned tubes is

$$\Delta P_{tube} = 1.78 \times 10^5 \text{ Pa}$$

$$= 1.25 \text{ psi}$$

The pressure drop due to friction on the shell side of the heat exchanger is given by

$$\Delta P_{sh} = \frac{(G_{sh})^2}{2gC_{p,a}} 4f_{sh}\frac{L_{sh}}{D_{sh}} \quad \text{(B21)}$$

For HX-1 with a shell side pressure of approximately 5.52×10^5 Pa (80 psia), the computed pressure loss is

$$\Delta P_{sh} = 2.83 \times 10^3 \text{ N/m}^2$$

$$= 0.41 \text{ psi}$$

And for HX-2 with a shell side pressure of approximately 3.31×10^6 Pa (480 psia), the computed pressure loss is

$$\Delta P_{sh} = 4.65 \times 10^2 \text{ Pa}$$

$$= 0.067 \text{ psi}$$

In the cycle analysis presented, the heat exchanger losses were assumed to be 1 percent of the respective inlet stream pressures. The above computed pressure drops for the finned tube heat exchanger configuration described in this appendix are all less than 1 percent. However, the absolute differences between the assumed and computed heat exchanger pressure losses are rather small. Thus, the effect of these differences on the cycle results presented in the report is insignificant.

References

1. An International Research and Development Program for LH_2-Fueled Aircraft. DFVLR (Germany), Hydrogen in Air Transportation Ad Hoc Executive Group, July 1980.
2. Witcofski, R. D.: Comparison of Alternate Fuels for Aircraft. NASA TM-80155, Sept. 1979.
3. Brewer, G. D.; and Morris, R. E.: Study of LH_2-Fueled Subsonic Passenger Transport Aircraft. (LR-27446, Lockheed-California Co.; NASA Contract NAS1-12972.) NASA CR-144935, Jan. 1976.
4. Whitlow, J. B., Jr.; Civinskas, K. C.; and Weber, R. J.: Preliminary Appraisal of Hydrogen and Methane Fuel in a Mach 2.7 Supersonic Transport. NASA TM X-68222, 1972.
5. Miller, B. A.: Analysis of Several Methane-Fueled Engine Cycles for Mach 3.0 Flight. NASA TN D-4699, July 1968.
6. Hendricks, R. C.; Baron, A. K.; and Peller, I. C.: GASP—A Computer Code for Calculating the Thermodynamic and Transport Properties for Ten Fluids: Parahydrogen, Helium, Neon, Methane, Nitrogen, Carbon Monoxide, Oxygen, Fluorine, Argon, and Carbon Dioxide. NASA TN D-7808, Feb. 1975.
7. Fishbach, L. H.; and Caddy, M. J.: NNEP—The Navy-NASA Engine Program. NASA TM X-71857, Dec. 1975
8. Hendricks, R. C.; Peller, I. C.; and Baron, A. K.: WASP—A Flexible Fortran IV Computer Code for Calculating Water and Steam Properties. NASA TN D-7391, Nov. 1973.
9. Onat, E.; and Klees, G. W.: A Method to Estimate Weight and Dimensions of Large and Small Gas Turbine Engines. NASA CR-159481, Jan. 1979.
10. Kays, W. M.; and London, A. L.: Compact Heat Exchangers. The National Press, 1955.
11. McCarty, R. D.; and Weber, L. A.: Thermophysical Properties of Parahydrogen From the Freezing Liquid Line to 5000° R for Pressures to 10 000 psia. (NBS-TN-617, National Bureau of Standards; NASA order T-1813-A.) NASA CR-127701, Apr. 1972.
12. Hilsenrath, J.: Tables of Thermodynamic and Transport Properties of Air, Argon, Carbon Dioxide, Carbon Monoxide, Hydrogen, Nitrogen, Oxygen, and Steam. Pergamon Press, 1960.
13. McAdams, W. H.: Heat Transmission. 3rd ed., McGraw-Hill Book Co., Inc. 1954.
14. Kreith, F.: Principles of Heat Transfer. 2nd ed., International Textbook Co., 1965.
15. Heat Exchanger Tube Manual. 3rd ed., Scovill Manufacturing Co., 1957.

1. Report No.	2. Government Accession No.	3. Recipient's Catalog No.
NASA TP-2294		

4. Title and Subtitle

Analysis of a Topping-Cycle, Aircraft, Gas-Turbine-Engine System Which Uses Cryogenic Fuel

5. Report Date: April 1984

6. Performing Organization Code

7. Author(s)

George E. Turney and Laurence H. Fishbach

8. Performing Organization Report No.: E-1735

10. Work Unit No.

9. Performing Organization Name and Address

National Aeronautics and Space Administration
Lewis Research Center
Cleveland, Ohio 44135

11. Contract or Grant No.

13. Type of Report and Period Covered: Technical Paper

12. Sponsoring Agency Name and Address

National Aeronautics and Space Administration
Washington, D.C. 20546

14. Sponsoring Agency Code

15. Supplementary Notes

Presented in part at AIAA Aircraft Systems and Operational Meeting, Fort Worth, Texas, Oct. 17-19, 1983.

16. Abstract

An analytical investigation was made of a topping-cycle aircraft engine system which uses a cryogenic fuel. This system consists of a main turboshaft engine that is mechanically coupled (by cross-shafting) to a topping loop, which augments the shaft power output of the system. The thermodynamic performance of the topping-cycle engine was analyzed and compared with that of a reference (conventional) turboshaft engine. For the cycle operating conditions selected, the performance of the topping-cycle engine in terms of brake specific fuel consumption (bsfc) was determined to be about 12 percent better than that of the reference turboshaft engine. Engine weights were estimated for both the topping-cycle engine and the reference turboshaft engine. These estimates were based on a common shaft power output for each engine. Results indicate that the weight of the topping-cycle engine is comparable with that of the reference turboshaft engine.

17. Key Words (Suggested by Author(s))

Topping cycle
Aircraft propulsion system
Aircraft engine system

18. Distribution Statement

Unclassified - unlimited
STAR Category 07

19. Security Classif. (of this report)	20. Security Classif. (of this page)	21. No. of pages	22. Price*
Unclassified	Unclassified	22	A02

*For sale by the National Technical Information Service, Springfield, Virginia 22161

NASA-Langley, 1984

4 1 1U,A, 840409 S00903DS
DEPT OF THE AIR FORCE
AF WEAPONS LABORATORY
ATTN: TECHNICAL LIBRARY (SUL)
KIRTLAND AFB NM 87116